EFFECTS OF BUILD ORIENTATION AND THICKNESS OF ALLOWANCE ON THE FATIGUE BEHAVIOUR OF 15-5 PH STAINLESS STEEL MANUFACTURED BY DMLS

Dario Croccolo [1], Massimiliano De Agostinis [1], Stefano Fini [1], Giorgio Olmi [1], Nebojsa Bogojevic [2], Snezana Ciric-Kostic [2]

[1] Department of Industrial Engineering (DIN), University of Bologna, Bologna, Italy

[2] Faculty of Mechanical and Civil Engineering in Kraljevo, University of Kragujevac, Serbia

Corresponding Author:

Eng. Giorgio Olmi, Ph.D.

Department of Industrial Engineering (DIN)

University of Bologna

Viale del Risorgimento, 2 - 40136 BOLOGNA (BO) - ITALY

Phone: +39 051 2093455, +39 0543 374427 (in Forlì)

Fax: +39 051 2093412

E - mail: giorgio.olmi@unibo.it

ABSTRACT

The present study is focused on the fatigue strength of 15-5 PH stainless steel, built by Direct Metal Laser Sintering. Six-specimen sets were manufactured, mechanically and thermally treated and tested under rotating bending fatigue. The study investigates the effects of the build orientation (parallel, perpendicular, or 45° inclined with respect to the vertical stacking direction) and of allowance for machining (1mm or 3mm at gage). The results, processed by an ANOVA methodology, indicate that allowance for machining has a beneficial effect on the fatigue response. Removing the surface irregularities, averagely leads to a 19% enhancement of the fatigue limit. The build orientation also becomes beneficial, when the slanted samples are included in the experiment. In this case, a fatigue strength increase up to 20% can be achieved. Further developments will include the investigation of the effects of heat and surface treatments, involving also further materials in the study.

Keywords: Rotational Bending, Fatigue strength, Stainless steel, Direct Metal Laser Sintering, Build orientation, Allowance for Machining.

NOMENCLATURE

AM	Additive Manufacturing
ANOVA	Analysis of Variance
CAD	Computer Aided Design
CTE	Coefficient of thermal expansion
DMLS	Direct Metal Laser Sintering
FL	Fatigue Limit [MPa]
H,1	Horizontally oriented specimens with 1mm allowance for machining (Set #1)
H,3	Horizontally oriented specimens with 3mm allowance for machining (Set #4)
M_b	Bending Moment [Nm]
R	Stress Ratio (fatigue tests)
f	Frequency (fatigue tests) [Hz]
R_a	Roughness Average [μm]
R^2	Linear Correlation Coefficient
S,1	Slanted specimens with 1mm allowance for machining (Set #3)
S,3	Slanted specimens with 3mm allowance for machining (Set #6)
S_i	10-base logarithm of σ_i
$\overline{S_{i.}}$	(i-th) row mean (for ANOVA)
$\overline{S_{.j}}$	(j-th) column mean (for ANOVA)
$\overline{S_{..}}$	Overall mean (for ANOVA)
SLM	Selective Laser Melting
S-N curve	Maximum Bending Stress vs. Life Cycles curve in the finite life domain
SSBC	Sum of Squares between Columns (for ANOVA)
SSBI	Sum of Squares Interaction (for ANOVA)
SSBR	Sum of Squares between Rows (for ANOVA)
UTS	Ultimate Tensile Strength [MPa]
V,1	Vertically oriented specimens with 1mm allowance for machining (Set #2)
V,3	Vertically oriented specimens with 3mm allowance for machining (Set #5)
σ_i	Finite life fatigue strength for the (i- th) sample set

INTRODUCTION

Nowadays, there is an increasing interest towards Additive Manufacturing (*AM*) techniques, as this technological process is potentially capable of producing even complexly shaped parts in a relatively short time [1-2]. In addition, the parts can be easily built, with a high level of flexibility, starting from a *CAD* model [3-5]. *AM* offers further advantages arising from a faster time-to market, a high efficiency in material utilization with a particularly reduced powder waste [6]. A possible drawback of *AM* techniques consists in the residual stresses that may be generated during part building. Therefore, suitably shaped supports are usually applied to safely attach the built part to a rigid base-plate, thus preventing its movements through the powder bed or distortions induced by the residual stress field [3]. Moreover, *AM* produced parts are likely to be affected by defects, being often due unmolten particles, entrapped gas bubbles, or missing fusion [6-7]. A poor surface finishing with high roughness may also arise from the powder adjacent to the fabricated area being partially sintered and attached to the part surface due to heat transfer in the neighborhood of the fabrication area [8]. Direct Metal Laser Sintering (*DMLS*) by EOS and Selective Laser Melting (SLM) by MTT Technologies Group can be mentioned among the most important AM processes for metals [5]. A possible difference between the two technologies lies in the mechanism that makes the powder fuse together. In the case of SLM a full melting is achieved, whereas in the case of DMLS, selective laser sintering causes the powder to fuse together. Anyway, nowadays they can be regarded as basically the same technique, being grouped under the powder bed fusion technologies. They both have wide applications to metals, as pointed out in recent review studies [5, 9].

The aforementioned base-plate is usually placed on a horizontal plane, and the parts are generated along a vertical stacking direction. A number of studies, involving different materials and AM processes have been focused on the possible effect of the build direction on the mechanical static and fatigue responses of the manufactured parts. Some researchers investigated a possible influence of the angle between the main axis of inertia (namely, the longitudinal axis of the specimen) and the stacking direction on the part strength. Several studies were performed on selective laser melted Ti6-Al-4V samples. The results indicated that the build orientation may significantly affect the fatigue response, in particular the endurance strength in the finite life domain. A higher life for the same load entity was retrieved for the build orientation, where the layer plane is parallel to the loading axis [10]. A similar effect was also observed on fracture toughness [11]. The possible effect of the build direction on the fatigue response, considering both the fatigue limit and the fatigue strength in the finite life domain, was also the topic of a previous study by the same authors. This research involved MS1 Maraging steel parts, built, considering three different orientations, with post-manufacture mechanical and heat treatments. An experimental campaign led to the result that the fatigue response is not significantly affected by the build direction, since, for Maraging steels, post-manufacture treatments have a great role at removing sources of anisotropy [12].

Further research in the literature was focused on the mechanical behaviour of 15-5 PH stainless steel parts. This type of steel is commonly used in applications such as aircraft components, or for parts under high pressure or working in harsh corrosive environments, including valves, shafts, fasteners, fittings and gears [3, 13]. It must be pointed out that the 15-5 PH alloy has been developed, in order to achieve a greater toughness with respect to 17-4 PH. This outcome is fulfilled by a reduced content of delta ferrite and an accurate control of inclusion size and shape. In particular, it is well known that the volume fraction of Delta-Ferrite significantly affects the low-temperature toughness [14]. The precipitation of Fe-Cu in the Delta-Ferrite leads to aged hardening after long term aging with consequent decrease in elongation and embrittlement of 17-4 PH [15]. The current processing of 15-5 PH alloy ensures the minimization and control of the delta ferrite content, thus taking advantage of the precipitation mechanism, to enhance toughness [16]. The 15-5 PH stainless steel used in the present work is supplied as powder by EOS and is optimized for DMLS

application (and related post-processing), meeting all the Standard specifications regarding composition and mechanical properties as well as fracture toughness [17]. A lack of studies on the effect of the build direction on the fatigue properties of this steel can be pointed out. In particular, the research [3] was focused on the build orientation effect on the static response only. Experimental results indicated that this response is enhanced, when the load direction acts along the layer plane, but the fatigue properties for different build directions were not investigated. Additional studies [18-20] deal with the static properties of 17-4 PH stainless steel, focusing on the effects of build direction and microstructure. Comparison is also made to the mechanical response of wrought material. The study [21] is very interesting, as it can be mentioned as one of the few that deal with fatigue on 17-4 PH stainless steel, however, the fatigue response, even in the high cycle fatigue field, is studied by a strain-life model, which is usually better suited to low cycle fatigue. Moreover, just two build orientations are considered. Other studies are documented in [18-19], but are more oriented to the effects on technological issues like machinability, rather than to the outcomes on the fatigue strength. This point is attracting interest, considering also that the rough 'as built' surface often acts as a crack initiator under fatigue, therefore the fatigue strength is presumably affected by the surface condition and the design process must take this issue into account. For this reason, post-fabrication surface treatment methods have been developed and used to enhance the finishing of the built parts surface layers. On one hand, conventional methods, such as machining [22-23], mechanical polishing [24], abrasive flow polishing [25], chemical milling [26-27] and electroplating [24] have proved their efficiency. On the other hand, it must be argued that some of these techniques could be difficult to apply in presence of undercut, or of internal or complexly shaped surfaces. Electroplating has proved to be generally efficient from this point of view, but sometimes it may leave some residuals and small sharp-tip features on the treated surface, which may even worsen the mechanical properties. Electropolishing, where the treated part act as an anode, and, upon voltage application, is polished through the removal of surface particles, may be regarded as a valid and challenging alternative. The study [8] indicates that by a proper choice of the process parameters, such as current, voltage, electrode distance and treatment time, a significant beneficial drop of the surface roughness can be achieved.

The subject of this paper consists in an experimental study on the fatigue response of 15-5 PH stainless steel parts fabricated by the *DMLS* process. Two factors were considered: the build direction and the post-processing procedure. In particular, three different build orientations were considered, with different inclinations of the main axis of inertia of the parts with respect to the base plate. Regarding the post-processing procedure, the effect of allowance and subsequent machining, with different thicknesses of material to be removed was studied. This experimental plan derives its motivations from the previous study dealing with Maraging steel [12], which was focused on the effect of the build orientation, and from some recent studies, e.g. [11, 28-30], which are starting to investigate the effects of the amount of material to be removed after sintering on mechanical properties. However, in these papers, the size effect of the block, from which the part is machined, is studied from the point of view of fracture mechanics, whereas similar investigations dealing with high cycle fatigue properties are still missing. Moreover, the fatigue performance of machined Ti-6Al-4V samples with suitable selection of allowance has also been the topic of the study [31], which confirms the general interest in this topic. Issues of novelty also arise from considering three orientations with respect to the vertical stacking direction: horizontal, vertical and slanted. The slanted orientation has been very rarely studied in the previous literature: in particular with reference to AlSi10Mg [32] and, partially, with reference to 17-4 PH stainless steel [33]. Conversely, no contributions tackle the study of the effect of build orientation, considered over three levels, on 15-5 PH stainless steel fatigue response.

MATERIALS AND METHODS

The experimental campaign was performed under rotating bending, following the ISO 1143 [34] Standard. Specimens were designed accordingly, with reference to the cylindrical smooth geometry (with uniform cross section at gage). The smallest dimension suggested by the standard, 6mm diameter at gage, was chosen as a good compromise between standard requirements and production costs. A drawing of the specimen is shown in Fig. 1, with indication of all its dimensions and tolerances. The chemical composition of 15-5 PH stainless steel (PH1 stainless steel by EOSGmbH – Electro Optical Systems, Krailling/Munich, Germany) is provided in Table 1 [17].
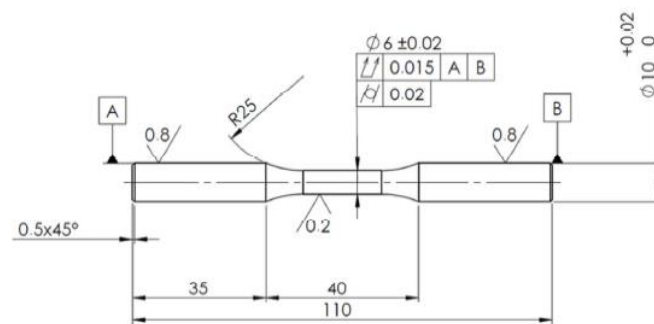

Fig. 1: Specimen with 6 mm diameter at gage in agreement with ISO 1143 Standard [34]

The specimens were manufactured by EOSINT M280 system (EOS GmbH - Electro Optical Systems, Krailling/Munich, Germany), equipped with Ytterbium fibre laser with 200W power and emitting 0.2032mm thickness and 1064nm wavelength infrared light beam. The process takes place in an inert environment and the scanning speed may range up to 7000 mm/s. The machine features a working space with 250 × 250 mm dimensions on the horizontal plane and a maximum height of 325 mm. The applied process parameters were defined according to the EOS Part Property Profile named "Surface". In particular, the layer thickness was set to 20 μm and a parallel scan strategy with alternating scan direction was adopted. For the subsequent layers the scanning direction was rotated by approximately 70°, in order to prevent or reduce in-plane property variations. Some examples of the scanning patterns are shown in Fig. 2, where arrows indicate the different scan directions at different stages of production and on different layers. A contour line was finally scanned, in order to complete the part shaping and to make its external surface as smoother as possible [35].

Table 1: Chemical composition of 15-5 PH1 Stainless Steel by EOS

Cr [%]	Ni [%]	Cu [%]	Mn [%]	Si [%]	Mo [%]	Nb [%]	C [%]	Fe [%]
14-15.5	3.5-5.5	2.5-4.5	≤ 1	≤ 1	≤ 0.5	0.15-0.45	≤ 0.07	Balance

All the specimens underwent surface cleaning by micro-shot-peening, in order to close the pores that may be induced by laser sintering. According to the machine manufacturer [17], and in general for selective laser sintered parts [36], a 99% density can be achieved proceeding this way. Afterwards, the H900 heat treatment was performed [3, 17], thus following the recommendations by EOS. For this purpose, the samples were kept at the temperature of 482°C for 2 hours after a ramp increase (from the room temperature) in 1 hour time. This treatment, which is aimed at reducing the residual stresses, thus enhancing the fatigue response of the built parts, was performed with the samples being still connected to their supports, in order to prevent them from bending. Finally, the specimens underwent machining and refining by grinding with the aim of accomplishing the roughness and dimensional specifications and of improving the fatigue performance.

Six specimen sets were manufactured: those of types #1 and #4 were built while lying horizontally on the base plate, therefore the angle between their longitudinal axis and the vertical stacking direction was 90°. Whereas, those of types #2 and #5 were built while standing vertically: in this case, the angle between their main axis of inertia and the stacking direction was 0°. Finally, the samples of sets #3 and #6 were built along a 45° inclined direction with respect to the base plate, so that the angle between their longitudinal axis and the vertical stacking direction was 45°. The difference between the samples of sets #1 and #4 is that the first ones were produced with the same shape as shown in Fig. 1, with a 1mm uniform allowance both at the gage (diameter increased from 6 to 8 mm) and at the heads (diameter increased from 10 to 12 mm). The samples were then machined to meet the drawing specifications, regarding both dimensions and roughness. Conversely, the samples of set #4 were built with a cylindrical shape with 12 mm diameter over their entire length. It implies that the allowance was 1mm at the heads and 3mm at the specimen gage. These samples also went through machining to meet the same specifications as in Fig. 1: therefore, a higher thickness of material was removed at the gage with respect to the samples of type #1. The same difference applies also to sets #2-#3 (built with uniform allowance and reduced section at gage) and #5-#6 (built with cylindrical layout).
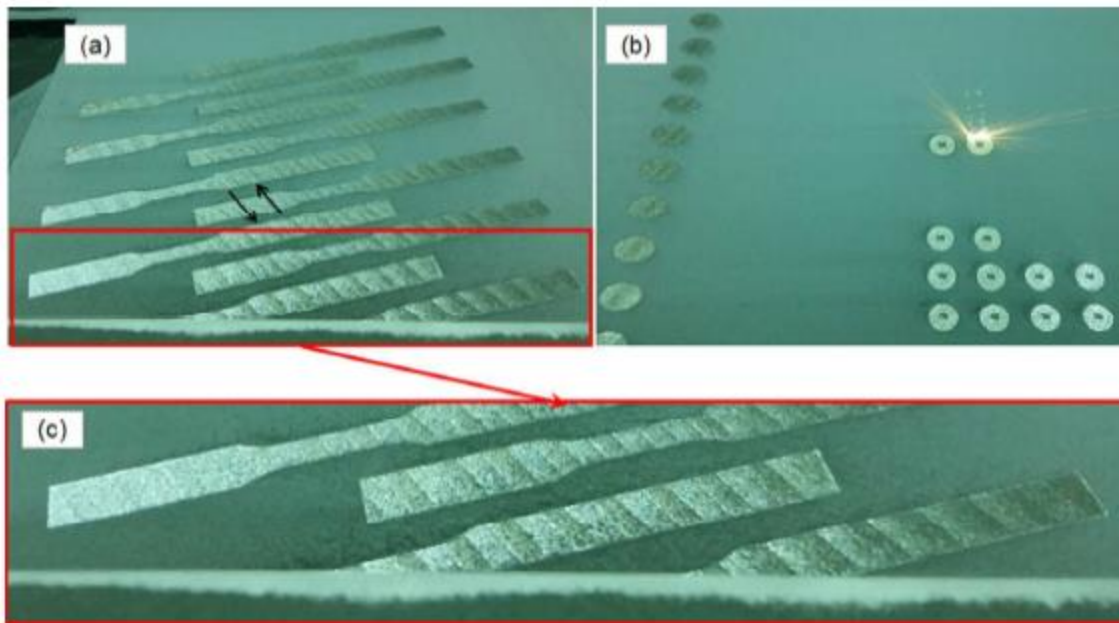

Fig. 2: Some examples of the scanning patterns, as the specimens lying horizontally (a) and standing vertically (b) are being built (arrows indicate the scan directions), (c) zoomed image, where powder residuals are clearly visible at the bottom side (close to the door chamber), around the sample contours and as darker stripes on the built areas

The described experimental plan can be regarded as a 2-factor experiment: the first factor, build orientation, was investigated over three levels (horizontal, vertical and slanted), whereas the second one, allowance (material thickness to be removed by machining) was considered at two levels (1 mm and 3mm at gage). This experimental plan is summarized in Table 2, with indication of sample set numbers and of short names to be used in the following. Each set was composed by 7 to 10 samples (the number of samples for each set is also reported in Table 2), considering that some samples were unfortunately damaged during manufacturing. Regarding this point, it is worth mentioning that residual stresses were presumably particularly high, following the building stage. As a result of this, some samples got bended and therefore permanently deformed. It should be pointed out that such large deformations had not been observed in the previous study dealing with Maraging steel [12], so it indicates that stainless steel is particularly sensitive to the generation of process induced residual stresses. In order to get a full

comprehension of this outcome, consistent with the results presented in [37], a brief resume of the process that leads to the residual stress state generation is provided below.

Table 2: Experimental plan involving 2 factors (at 3 and 2 levels) and 6 treatment combinations

		Thickness of allowance for machining	
		1 mm	3 mm
Orientation of the longitudinal axis of the sample (during the building process)	Horizontal	Set #1 (H,1): 7 samples	Set #4 (H,3): 9 samples
	Vertical	Set #2 (V,1): 10 samples	Set #5 (V,3): 10 samples
	Slanted	Set #3 (S,1): 10 samples	Set #6 (S,3): 9 samples

The residual stress state arises from the thermal cycle during the deposition and solidification and cooling of the material. The underlying mechanism is well highlighted in [38], where it is pointed out that, if thermal stresses exceed the yield stress, residual stresses are expected to remain after cooling and their sign turns to be the opposite of the sign of the thermal stresses. As the laser beam heats and melts the solid material, it tends to expand, but the thermal expansion is partially prevented by the surrounding colder material, which leads to a compressive thermal stress, generally exceeding the material yield point that is often reduced by the high temperature [39]. Afterwards, as the laser beam leaves that area, the irradiated zone cools and tends to shrink. Partial constraint by the solidified material of the layer underneath induces a tensile residual stress state that may even lead to macroscopic curvature of the fabricated part [39].

The number and thickness of the layers is likely to significantly affect the mechanism of residual stress generation [40]. The described mechanism occurs for each layer and especially in the case of many thin layers large tensile residual stresses accumulate inside the manufactured component [41]. This point provides a first explanation for the greater sensitivity of Stainless steel to residual stresses than Maraging steel, considering that in the first case the thickness layer is one half (20 µm) than for the latter (40 µm). A further explanation, mainly related to material physical properties, arises from the point that the coefficient of thermal expansion (CTE) has a large effect on the residual stress field generation. The higher CTE, the higher residual stresses. The CTE of Maraging steel is $10.1 \cdot 10^{-6}$ K^{-1}, whereas that of Stainless steel is $11.3 \cdot 10^{-6}$ K^{-1}, i.e. 12% incremented [40]. The gradient of CTE is also important: a recent study [42] has pointed out that the difference of CTE between different phases for the same material is likely to remarkably affect the residual stress field. For stainless steel, a not uniform state of heating/cooling along with a high number of thin layers may in turn strengthen this detrimental effect.

The adopted countermeasures against residual stresses consisted in carefully following the recommendations by EOS, guaranteeing as larger as possible contact between the samples and the base plate (to improve heat dissipation). Moreover, the largely deformed section, usually located at an extremity of the sample, was cut away. Moreover, in some cases, the samples were discarded and rebuilt, following the aforementioned recommendations. As mentioned above, the aging treatment was performed on all the samples, to drop down the residual stress state. Some stages of production, with reference to some of the aforementioned sample sets, are shown in Fig. 3. In particular, the significant bending that occurred in samples of Set #3 (S,1) is highlighted in Fig. 3 (d, e). In this case, deformation was concentrated at the ends

(whereas the remaining part was straight) and the heads were longer than the specifications in Fig. 1. Consequently, the deformed part could be cut upon machining.
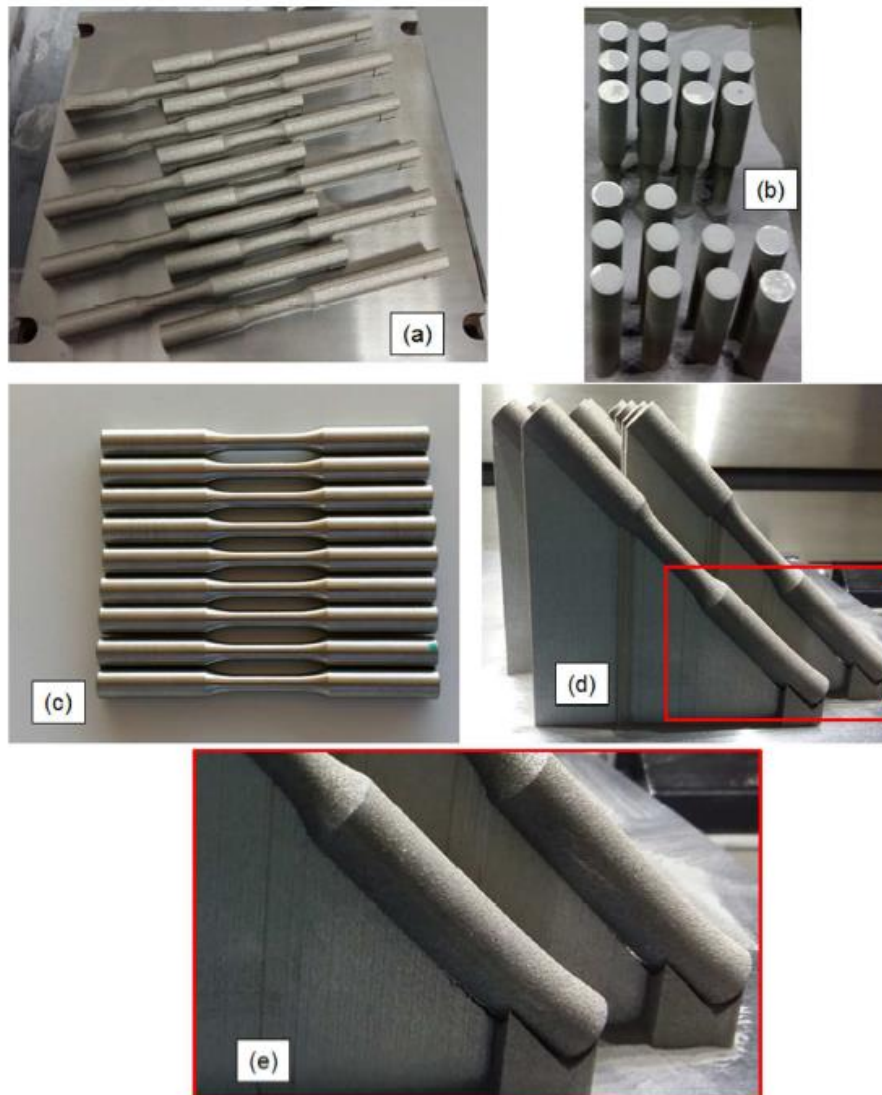

Fig. 3: *Some stages of sample production: (a) Set #1 (H,1) samples just after DMLS manufacturing and before the heat treatment, (b) Sets #2 (V,1) and #5 (V,3) samples during residual powder removal with internal gage (top) and cylindrical shape (bottom), (c) Set #4 (H,3) samples after machining and finishing, just before the beginning of the fatigue campaign, (d, e) Set #3 (S,1) samples before support detachment, bending highlighted in the detail view*

The fatigue campaign made it possible to obtain the S-N curves and the fatigue limits (*FL*s). A staircase method was applied to determine the *FL*: for this purpose, the series of failure and not-failure events was processed by the Dixon method [43-46]. A life duration of 10^7 cycles was set as run-out, based on the few available data on the fatigue response of sintered 15-5 PH stainless steel [3]. The Dixon method is an abbreviated staircase method that makes it possible to estimate *FL* even from a short series of nominal trials at staircase (four to six in this work). A confidence analysis (90% confidence level) was also performed based on the standard deviation of *FL* (scattering of the experimental results) and on the size of the sequence that led to its computation. The data in the finite life domain were processed according to the Standard ISO 12107 [47]: the stress and life were linearly interpolated in logarithmic coordinates. The lower and upper limits of the *S-N* curve have been determined, based on the standard deviation of the logarithm of the fatigue life. Respective failure probabilities of 10% and 90% were considered together with a 90% confidence level.

EXPERIMENTAL PROCEDURE

All the samples were initially measured, in order to check the dimensions and roughness specifications. For this purpose, a micrometer screw gage, a digital caliper (both with the resolution of 0.01mm) and a portable surface roughness tester (with the resolution of 0.01 µm, Handysurf E-30A; Carl Zeiss AG, Oberkochen, Germany) were used. The heads at both ends and the sample gages were measured at 90° angled points with 4 replications. Similar measurements were performed on specimen gages with 6 replications. The results are collected in Table 3 with reference to Set #2 (V,1). Regarding roughness, R_a has also been measured, considering 90° angled points around full diameters at both specimen heads with 8 replications. Similar measurements were then carried out at the gages. However, these measurements could not be carried out before fatigue testing because of the impossibility of correctly holding the tester detector above the specimen cylindrical surface for a sufficiently long longitudinal scan. Therefore, roughness measurements at gauges have been performed only after breakage on the specimens that experienced failures during the fatigue campaign. Consequently, not all the samples underwent this measurement, however the retrieved amount of data was sufficiently relevant to check the fulfilment of roughness specifications. The averaged values, where available, are included as well in the same Table. The results regarding the other sample sets are not reported for the sake of synthesis. All the yields are generally well consistent with the requirements in ISO 1143 [34] and with drawing specifications. The samples were also checked for hardness: HRC Rockwell hardness was determined on all the samples with three replications. The average values, ranging from 42 to 43.5 HRC, confirm an Ultimate Tensile Strength (*UTS*) from 1325 to 1375 MPa, which is in the order of that indicated in [17, 48-49] of 1310 MPa.

Table 3: *Dimensional and roughness measurement outcomes considering the samples of Set #2 (V,1)*

Specimen ID	Gage diameter			Head diameter (right side)			Head diameter (left side)		
	Mean [mm]	St dev. [mm]	Roughness [µm]	Mean [mm]	St dev. [mm]	Roughness [µm]	Mean [mm]	St dev. [mm]	Roughness [µm]
2.1	6.03	0.035	0.400	10.01	0.005	0.38	10.01	0.003	0.40
2.2	6.01	0.029	0.323	10.01	0.002	0.30	10.01	0.002	0.34
2.3	6.02	0.036	0.413	10.01	0.004	0.31	10.01	0.003	0.36
2.4	5.98	0.044	0.246	10.01	0.005	0.41	10.01	0.002	0.33
2.5	6.02	0.027	0.425	10.01	0.003	0.35	10.01	0.003	0.37
2.6	6.00	0.026	0.338	10.00	0.002	0.35	10.01	0.003	0.32
2.7	6.01	0.035	X	10.01	0.002	0.37	10.01	0.004	0.40
2.8	6.02	0.036	0.340	10.00	0.003	0.35	10.00	0.003	0.33
2.9	6.01	0.025	0.370	10.00	0.003	0.36	10.00	0.003	0.34
2.10	6.00	0.038	0.308	10.00	0.010	0.44	10.00	0.011	0.42

The specimens were tested under rotating bending fatigue by a rotary bending testing machine, where the specimen is loaded in the four-point bending configuration, so that bending moment M_b keeps constant over the entire sample length, and in particular at its gage [43]. The sample was clamped at its ends by a pressure of approximately 70 MPa [50-51]. All the tests were conducted under fully reversed bending load (stress ratio R =- 1) at the frequency f of 60 Hz.

At the end of the experimental campaigns, crack surfaces were carefully analysed by a stereo microscope for the individuation of the crack nucleation point and of the zones of stable and unstable crack propagation. Some samples were cut and resin embedded. In particular, transverse sections of the specimen at the gages and longitudinal sections at the heads were considered. Fractographic and micrographic analyses were then performed with the aim of investigating the possible presence of porosities, inclusions, spots of oxides and micro-cracks. For this purpose, a Stemi 305 stereo-microscope (by ZEISS, Oberkochen, Gernany) has been utilized for fractographies, whereas an Optiphot-100 optical microscope (by Nikon, Melville, NY, United States) has been applied for both micrographic and (more

zoomed) fractographic analyses. In the case of micrographies, chemical etchings were performed by the following solution for a duration of 30s after heating in oven up to 90°C. 20 ml of Glycerol ($C_3H_8O_3$) were mixed with 10 cc of Nitric Acid (HNO_3), then 20 cc of Chloridric Acid (HCl) were mixed with 10 cc of Hydrogen peroxide (H_2O_2). Afterwards, these two compounds were merged together (50%-50% ratio) befo-

Table 4: Data retrieved from the tests on all the sample types

Specimen ID	Stress [MPa]	Life [N]	Failure
1.1	420	---	N
1.2	550	144,726	Y
1.3	524	167,829	Y
1.4	500	---	N
1.5	500	728,708	Y
1.6	475	8,423,284	Y
1.7	651	47,315	Y
2.1	651	4,834,809	Y
2.2	711	1,871,476	Y
2.3	590	108,926	Y
2.4	590	68,686	Y
2.5	470	---	N
2.6	560	43,729	Y
2.7	530	---	N
2.8	560	2,807,208	Y
2.9	530	2,564,861	Y
2.10	500	5,047,111	Y
3.1	640	---	N
3.2	670	8,344,160	Y
3.3	640	---	N
3.4	670	---	N
3.5	700	---	N
3.6	880	573,080	Y
3.7	730	9,012,402	Y
3.8	790	4,974,052	Y
3.9	820	1,776,278	Y
3.10	850	497,854	Y
4.1	680	---	N
4.2	711	3,274,162	Y
4.3	680	---	N
4.4	711	8,364,965	Y
4.5	680	---	N
4.6	800	183,582	Y
4.7	770	368,551	Y
4.8	740	297,241	Y
4.9	740	2,850,771	Y
5.1	650	6,082,766	Y
5.2	711	7,366,205	Y
5.3	800	532,725	Y (NOT VALID)
5.4	590	---	N
5.5	620	1,256,019	Y (NOT VALID)
5.6	620	8,932,232	Y
5.7	590	---	N
5.8	620	6,397,216	Y
5.9	800	260,944	Y
5.10	770	503,334	Y
6.1	790	981,210	Y
6.2	820	459,548	Y (NOT VALID)
6.3	730	645,013	Y (NOT VALID)

re starting etching. Some micrographs were specifically devoted to the investigation of the actual microstructure, following the building process and the heat treatment. For this purpose, an additional set of specimens was manufactured: they had horizontal orientation and 1 mm allowance, like those of Set #1 (H,1), but did not undergo machining. Upon support detachment, it was therefore possible to individuate the orientation of the build planes and to perform cutting in parallel and perpendicular directions.

RESULTS

The results of the fatigue tests, involving all the sample sets are collected in Table 4: in particular, the sample identifier, the load level, in terms of the nominal stress at gage, and the observed life are reported. The final outcome of each trial is reported as well: "Y" indicates that failure occurred, whereas "N" indicates that the sample did not break down and the test was stopped upon the runout of 10 million cycles.

In the case of failure, it was of course checked that specimen separation had regularly occurred at the gage. Afterwards, the fracture surfaces were observed, to make sure that a fatigue initiation and propagation mechanism was actually responsible of the observed failure. Most failures regularly occurred at gage, but in some cases, for sample sets #4 (H,3) and #6 (S,3), unusual and unexpected failures at specimen heads were observed: one of them is depicted in Fig. 4. It must be remarked that this outcome is not completely new, as it had also been observed in the previous research regarding Maraging steels. In that study, an analysis by dye penetrants had indicated the presence of some spots of unconformable roughness, which were likely to have triggered the crack in combination with the clamping pressure. In the present study, the roughness at sample ends was carefully checked by multiple measurements and was found to be consistent with the specifications. These results were not considered for further processing (tagged as "NOT VALID" in Table 4) and the possible reasons for these occurrences were later investigated by fracto-graphic and micrographic analyses.

Fig. 4: Unexpected failure at sample head

DISCUSSION

The results reported in the previous Section were initially processed, in order to determine the fatigue curves in the finite life domain. The S-N curves were retrieved as linear regressions in double logarithmic scale: they are plotted in Fig. 5 with reference to horizontal, vertical and 45° inclined samples with 1 mm allowance (Sets #1 to #3) and in Fig. 6 for the other sample sets with 3 mm allowance (Sets #4 to 6). For the sake of clarity, short names are appended to the sample set numbers. The maximum likelihood bands at the 90% confidence level and the experimental data are included as well in the graphs. The experimental results can be generally well interpolated by a linear regression line with a linear correlation coefficient (R^2) up to 0.8. The corresponding equations, related to 50% probability of failure Basquin fatigue curves, are provided in Eqs. (1) to (6), respectively for Sets #1 to 6. σ_i indicates finite life fatigue strength for the (i-th) set.

$$\sigma_1 = 1,323 \cdot N^{-0.07} \tag{1}$$

$$\sigma_2 = 915 \cdot N^{-0.04} \tag{2}$$

$$\sigma_3 = 2,850 \cdot N^{-0.09} \tag{3}$$

$$\sigma_4 = 1,208 \cdot N^{-0.03} \tag{4}$$

$$\sigma_5 = 2,242 \cdot N^{-0.08} \tag{5}$$

$$\sigma_6 = 2,161 \cdot N^{-0.07} \tag{6}$$

It can be emphasized that all the exponents are quite close to each other and varying in the interval -0.09 to -0.03, which indicates that all the curves have a similar slope and a horizontal-like trend. This outcome is

clearly related to the roughness level of the tested samples that ranges from 0.3 μm to 0.4 μm as an average, as reported in Table 3. The aforementioned roughness levels are quite close to those of the specimens of the same material, involved in the fatigue campaign [48-49], which led to well comparable results regarding the finite life domain curve and its slope. Conversely, the experimentations reported in [3] involved *SLM* built Stainless steel parts with an approximately 10-time higher roughness, and a much steeper curve involving a strong drop for increasing life was retrieved.
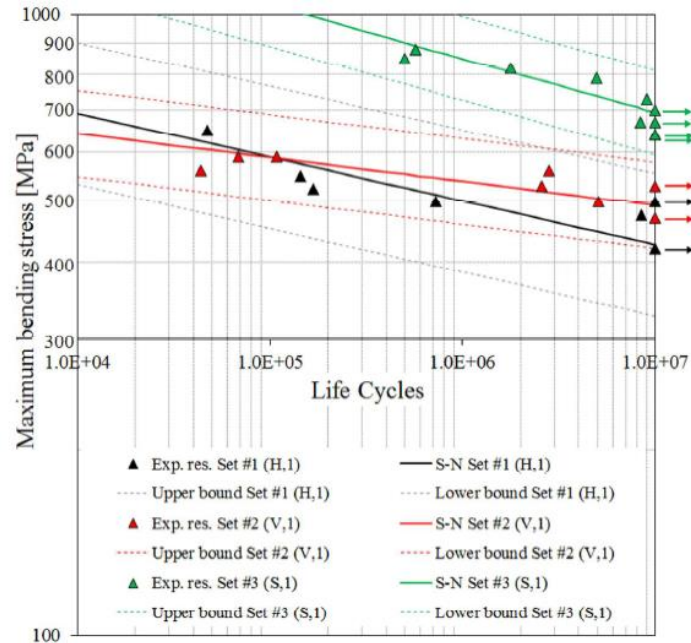
Fig. 5: *S-N curves for sample Sets #1 (H,1), #2 (V,1) and #3 (S,1) (arrows indicate run-outs): effect of the build orientation compared for reduced (1 mm) allowance for machining*
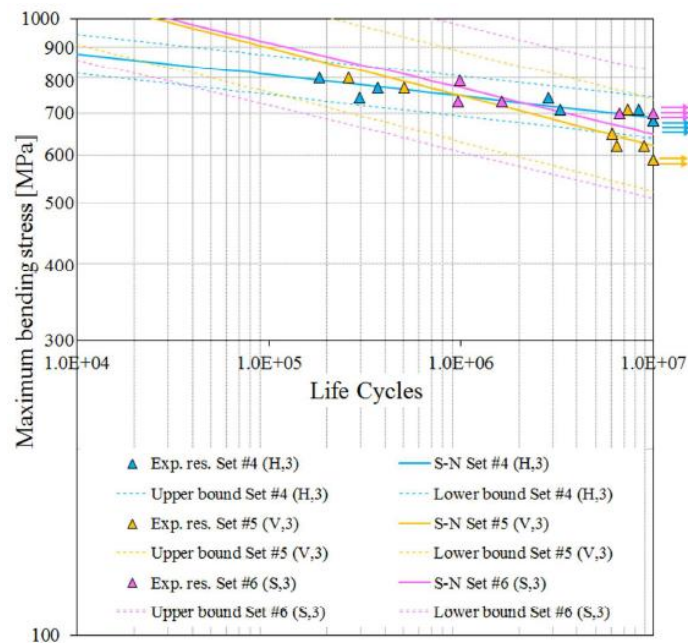

Fig. 6: *S-N curves for sample Sets #4 (H,3), #5 (V,3) and #6 (S,3) (arrows indicate run-outs): effect of the build orientation compared for incremented (3 mm) allowance for machining*

Observing the *S-N* curves in Fig. 5, referred to the lower allowance level, it can be remarked that those for horizontally and vertically built samples (Sets #1 and #2) are quite close, whereas that for the slanted ones (Set #3) is much higher, indicating a greater estimated strength for the same fatigue life. The analysis of the graph in Fig. 6, having the same axis scales as the previous one, indicates that the curves for the sets with

the upper allowance level (Sets #4 to #6) are quite close one another. Moreover, these curves generally correspond to a higher strength in the finite life domain with respect to those for lower allowance.

In order to better investigate the relationships among the six curves and the effects of the investigated factors, they were processed by the *ANOVA*-based statistical tool developed in [52]. We have extended this tool that was initially set-up for designs with just one factor to two-factor experiments, managing not only the main effects of the factors but also their interaction. As in the conventional ANOVA [53-54] for the comparison of distributions of yields, the differences between the curve trends have been here compared to the scattering of the experimental results. All the data have been processed in the logarithmic scale: in particular, S_i indicates the 10-base logarithm of σ_i, considering the fatigue curves in Eqs. (1)-(6). As a first step, row ($\overline{S_{1.}}$, $\overline{S_{2.}}$, $\overline{S_{3.}}$) and column ($\overline{S_{.1}}$, $\overline{S_{.2}}$) means have been computed, combining the functions in Eqs. (7) to (11).

$$\overline{S_{1.}} = \frac{S_1 + S_4}{2} \tag{7}$$

$$\overline{S_{2.}} = \frac{S_2 + S_5}{2} \tag{8}$$

$$\overline{S_{3.}} = \frac{S_3 + S_6}{2} \tag{9}$$

$$\overline{S_{.1}} = \frac{S_1 + S_2 + S_3}{3} \tag{10}$$

$$\overline{S_{.2}} = \frac{S_4 + S_5 + S_6}{3} \tag{11}$$

The overall mean was then computed as reported in Eq. (12):

$$\overline{S_{..}} = \frac{S_1 + S_2 + S_3 + S_4 + S_5 + S_6}{6} \tag{12}$$

The "Sum of Squares between Rows" (*SSBR*), i.e. the term related to the effect of the "Row" factor, namely the build orientation, was determined as the function in Eq. (13), where the sum of squares are weighted by the factor 2, considering that the row means are averaged between two functions.

$$SSBR = \left[\left(\overline{S_{1.}} - \overline{S_{..}} \right)^2 + \left(\overline{S_{2.}} - \overline{S_{..}} \right)^2 + \left(\overline{S_{3.}} - \overline{S_{..}} \right)^2 \right] \cdot 2 \tag{13}$$

The "Sum of Squares between Columns", *SSBC*, being related to the effect of the Column factor, i.e., of the allowance, was similarly determined as in Eq. (14), where the weight factor is 3, as an effect of the column means being averaged among three S-N functions.

$$SSBC = \left[\left(\overline{S_{.1}} - \overline{S_{..}} \right)^2 + \left(\overline{S_{.2}} - \overline{S_{..}} \right)^2 \right] \cdot 3 \tag{14}$$

Finally, the interaction term, *SSI*, was determined as in Eq. (15).

$$SSI = \left(S_1 - \overline{S_{1.}} - \overline{S_{.1}} + \overline{S_{..}} \right)^2 + \left(S_2 - \overline{S_{2.}} - \overline{S_{.1}} + \overline{S_{..}} \right)^2 + \left(S_3 - \overline{S_{3.}} - \overline{S_{.1}} + \overline{S_{..}} \right)^2 +$$
$$+ \left(S_4 - \overline{S_{1.}} - \overline{S_{.2}} + \overline{S_{..}} \right)^2 + \left(S_5 - \overline{S_{2.}} - \overline{S_{.2}} + \overline{S_{..}} \right)^2 + \left(S_6 - \overline{S_{3.}} - \overline{S_{.2}} + \overline{S_{..}} \right)^2 \tag{15}$$

Regarding *SSBR*, *SSBC* and *SSI*, the related functions were converted into scalars by the computation of their integral means over the life range investigated in the fatigue campaign, i.e. in the 10^4 to 10^7 interval. The error term was finally determined as the sum of the squares of the residuals between the actual experimental data and the related interpolating *S-N* curves.

All the data were then processed as a conventional two-factor *ANOVA*, provided that the sum of squares terms were scaled, dividing them by the related degrees of freedom. The outcome of this analysis is summarized in Table 5, where the p-values in the last column indicate that both the factors and their interaction are highly significant.

Table 5: *Analysis of variance considering a 3-by-2 experiment*

	Sum of Squares	Degrees of freedom	Sum of Squares after scaling	Fisher's ratio	p-value
Effect of the build orientation	0.0222	2	0.0111	17.04	$4.0 \cdot 10^{-5}$
Effect of the thickness of allowance for machining	0.0121	1	0.0121	18.52	$3.1 \cdot 10^{-4}$
Interaction	0.0156	2	0.0078	11.99	$3.4 \cdot 10^{-4}$
Error	0.0137	21	0.0007		

A further analysis, which considered just a 2-by-2 experiment, discarding the results for slanted samples, was then performed by the same tool. The outcome of this study is reported in Table 6: it is important to point out, that, considering horizontal and vertical orientations only, the build direction is no longer significant and so is interaction, whereas the allowance factor retains its high significance. This result confirms the effectiveness of thickness of allowance and indicates that significant differences arising from the build orientation appear only when the slanted samples are introduced into the analysis.

Table 6: *Analysis of variance considering a 2-by-2 experiment (horizontal and vertical build orientations only)*

	Sum of Squares	Degrees of freedom	Sum of Squares after scaling	Fisher's ratio	p-value
Effect of the build orientation	0.0004	1	0.0004	0.59	0.45
Effect of the thickness of allowance for machining	0.0253	1	0.0253	37.69	$1.9 \cdot 10^{-5}$
Interaction	0.0011	1	0.0011	1.65	0.22
Error	0.0101	15	0.0007		

The results of the trials at staircase were processed by the Dixon method and led to the estimation of the *FL*s collected in the bar graph in Fig. 7 (a), along with the related confidence bands. The limit for the sample type #1 (H,1) was estimated as 480 MPa, a well comparable value to that for type #2 (V,1), 507 MPa. The other limits for horizontally and vertically built samples with incremented allowance were conversely significantly higher: 701 MPa for type #4 (H,3) and 605 MPa for the fifth sample set (V,3). The determined limits for the slanted samples were very close each other: both around 690 MPa for low (Set #3, (S,1)) and high (Set #6 (S,3)) allowance.

It is interesting to compare the determined *FL*s to the *UTS* strength of the material [17, 48-49], considering that a commonly accepted ratio (*FL/UTS*) is approximately 50% for metallic materials [55]. For this reason, the level of 50% of the *UTS* is appended in the bar graph in Fig. 7 (a). The marginal means plot of the two factors, i.e. build orientation and allowance to be removed by machining, are provided in Fig. 7 (b). It can be remarked that the *FL*s for Sets #1 (H,1) and #2 (V,1) are quite close to each other and correspond to 37% and 39% of the *UTS*: these values are lower than 50%, but it is worth noticing they are about ten points higher than the corresponding ratios for Maraging steel [12]. Interestingly, the determined *FL*s for other sample sets are very close to the 50% threshold. This indicates that the fatigue response of the here studied material, 15-5 Stainless steel, is less sensitive to the additive manufacturing process than that of Maraging

steel. Moreover, the retrieved results indicate that the endurance performance can be further increased, by increasing allowance and optimizing the build orientation, thus making it well comparable to that for wrought material. In particular, removing the surface irregularities, averagely leads to a 19% enhancement of the fatigue strength, whereas, by the slanted orientation an increase up to 20% may be fulfilled with respect to horizontal/vertical layouts. These data may be useful as design recommendations for highly loaded parts under fatigue or for the general assessment of *AM* processed mechanical components.
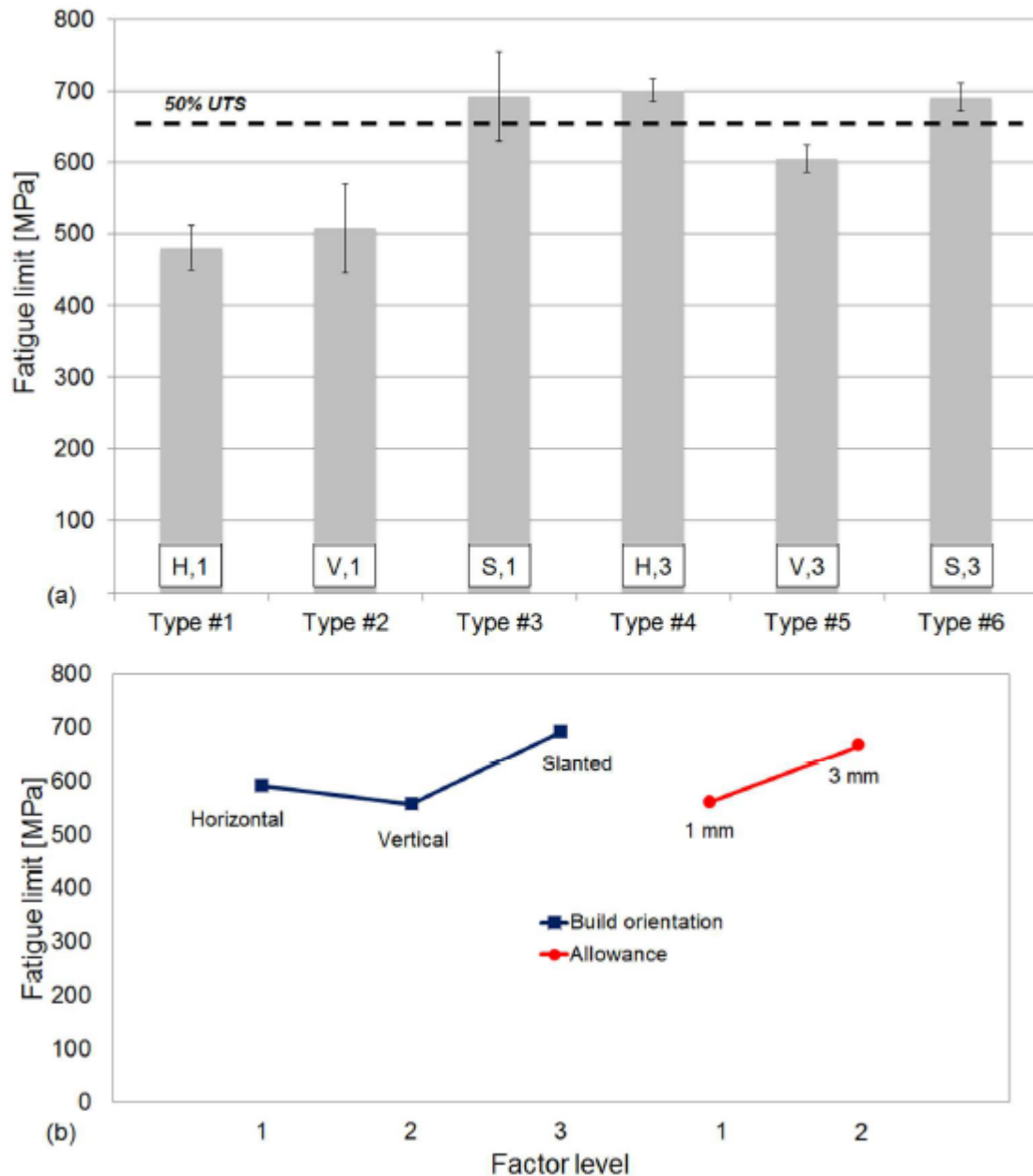
Fig. 7: *(a) Bar graph summarizing the fatigue limits for the six sample types along with their confidence bands; (b) The marginal means plot of the two factors*

The fatigue results in the infinite life domain confirm those for finite life and the outcomes of the previously reported analyses of variance. Regarding allowance, it is interesting to point out that machining the samples from oversized blocks leads to improved fatigue performance. A possible reason could be that the detrimental residual stress state is remarkably released by machining parts from a larger piece. The described outcome is presumably amplified for stainless steel, considering that this material is highly sensitive to residual stresses arising during the stacking process, as reported above. Moreover, performing machining from larger parts built by *AM* is able to cut surface defects. These irregularities are usually

concentrated at the surface layers, where, as remarked in the "Materials and Methods" Section, contour lines are scanned to complete the part shaping. These defects may be due to internal voids between the contour and the hatch, often arising from unmelted spots. These under surface irregularities may act as fatigue crack triggers, being thus responsible for the comparatively lower fatigue strengths in the case of the sets with low allowance. Conversely, removing the surface layers leads to a fatigue response that is well comparable to that of wrought material. This size effect is also confirmed also by the studies[11, 28-30], where a remarkably slower crack growth rate was observed, following machining from oversized blocks.

A further point regards the effect of build orientation, which becomes significant, only when slanted samples are introduced in the experiment. The negligible difference between the responses for horizontally and vertically built samples is well consistent with the results of the previous study [12] involving Maraging steel and can be interpreted in the frame of the effect of heat treatments removing the causes of anisotropy. Regarding slanted samples, it must be pointed out that very few results are reported in the literature: an experimental study [32] on AlSi10Mg also involved 45° inclined samples with respect to the base plate and to the load direction. After heat treatment, these samples showed good performance, compared to those with horizontal and vertical orientations. The response was the best at the highest load levels (in the finite life domain, for reduced life time). A possible interpretation is that irregularities due to missed scans, unmelted spots, or oxides, are usually concentrated on build planes. Following initiation, a crack tends to propagate along a perpendicular plane with respect to the load direction that is aligned with the sample longitudinal axis. Considering that the build planes are inclined with respect to the propagation plane, the notch effect arising from scan errors is therefore reduced. Moreover, should a crack propagate, the 45° inclined layers with respect to its pattern would act as barriers, thus reducing its propagation rate. It may be argued that similar considerations would also apply to horizontally built samples: in fact, the reduced notch effect, beneficially affecting their response, is often highlighted in the literature, for instance in [21, 32]. However, the build plane is much larger for horizontally built samples rather than for slanted ones, consequently the amount of defects spread over every single build plane is comparatively statistically much higher. This may also be due to a further phenomenon, related to the generation of metal residuals during production. Upon the scanning process, some amount of residual is made, as the result of burn out metal particles, and oxidation may be triggered during sparkling [56-57]. These particles are spread in the chamber and mixed with the new powder that is provided by the recoater and consequently also mixed on the bed surface during scanning. When a new layer is affected by these burn out residuals, if they are not suitably removed by the chamber air flow, spots of oxides and porosities may occur. The larger the surface being scanned, the larger the amount of residuals being generated, and consequently, the larger porosity occurrence. In addition, the number of defects per layer may be even incremented by the limited perpendicularity between the laser beam path and the build plane in conventional one-laser machines, due to the not optimal collocation of the fabricated part. This is also consistent with the outcomes in [21], where it is highlighted that, considering the overall volume of detected voids, horizontally built samples exhibit a higher level of porosity per unit volume. From this point of view, slanted samples can be seen as a good compromise between not high notch effect and low amount of defects in the build plane. As remarked in the Introduction, the fatigue performance of slanted samples had also been studied in [12] regarding Maraging steel and no significant improvements had been observed. It can be argued that the aforementioned remarks would not be sufficient to justify a different behaviour, when considering different material. A possible reason for the beneficial effect related to stainless steel is that the recommended (and applied) layer thickness is lower for stainless steel rather than for Maraging (20 μm vs. 40 μm). Consequently, the number of layers is comparatively higher (approximately the double) for the first one. Therefore, for stainless steel, reducing the number of defects per layer, while simultaneously keeping the notch effect low, becomes effective to improve the fatigue strength. Conversely, it is not significantly

effective for Maraging steel, for which the number of layers is much lower due to greater thickness. This outcome indicates that the obtained result, regarding the fatigue enhancement arising from the slanted orientation, keeps validity only for the studied material built with the described additive technology. In addition, it must be remarked that the fatigue response of the two materials has been assessed and is here compared, under the same most common manufacturing conditions, as they are the most recommended building strategies by EOS to optimize the part mechanical properties and productivity.
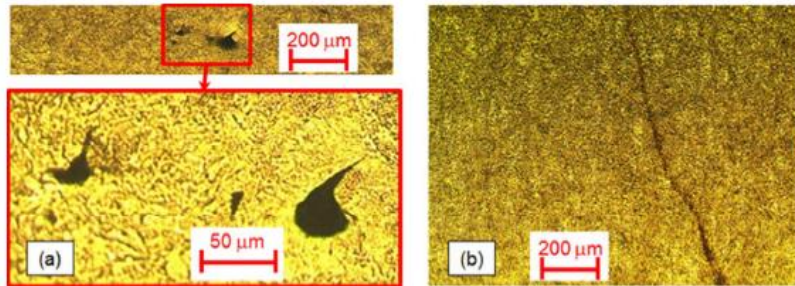
Fig. 8: *Micrographic analyses: (a) example of a void, (b) a transverse crack at the head of a samples of Set #5 (V,3) (all the images have been post-processed by microscope filters and polarized lenses)*

Finally, both fractographic and micrographic analyses have been performed on the broken samples to investigate the possible presence of voids, porosities, oxides or inclusions and to provide a reason for some cracks occurring at the head. In addition, micrographs have also been performed, in order to check the actual structure upon heat treatments on the build plane and in the stacking direction. The results indicate that some voids were sometimes observed, mainly at the heads: an example, retrieved by micrographic analysis, is depicted in Fig. 8 (a). These defects, together with the pressure transmitted by the fixture, are likely to have triggered some of the unexpected cracks at the heads, which then propagated along a transverse direction. It is interesting to remark that a transverse crack, shown in Fig. 8 (b), was detected on a specimen of Set #5 (V,3) that had regularly failed with separation at the gage. It indicates that another crack was propagating at the head, but failure at gage occurred earlier. Some samples of Set #6 (S,3) experienced failures at the head: these fracture surfaces have been carefully analysed by means of a stereo microscope and some images are available in Fig. 9 (a, b). An interesting point is that some spots of ferrous
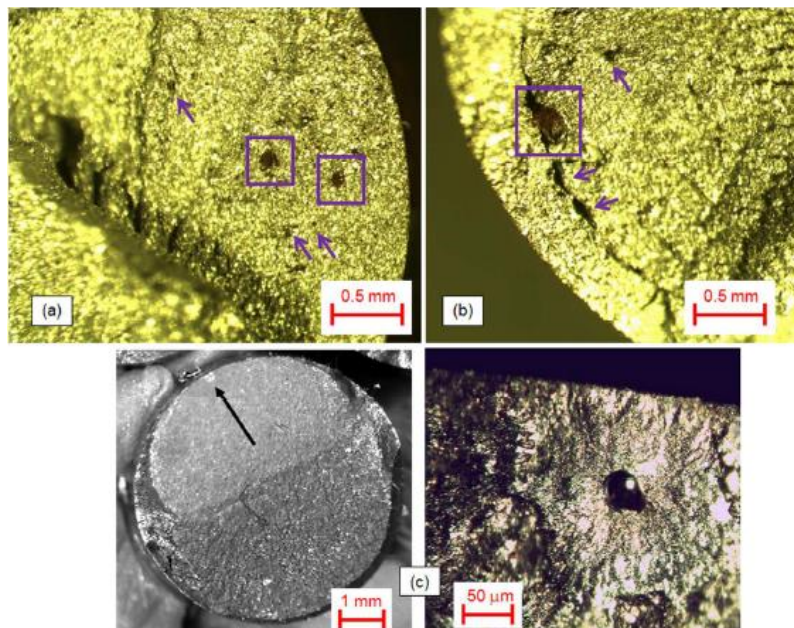

Fig. 9: *(a, b) Fracture surface analysis pointing out huge defects and spots of oxides (highlighted) that originated failure at the head in a sample of Set #6 (S,3) (post-processed images by microscope filters and polarized lenses), (c) regular failure at the gage, starting from a porosity (indicated by an arrow)*

oxides are present and are clearly visible due their brown colour. For the sake of clarity, they are also highlighted in the same pictures. Moreover, these oxides seem to have acted as crack inducers, as several cracks, approximately 250 μm long, appear to have started from these points. An interesting issue is that the studied material is a stainless steel, therefore, it is usually unexpected that oxides may occur. A possible reason is related to the aforementioned generation of residuals. An important role is played by the inert gas that flows in the chamber, from outlets placed at the rear side, towards the front of the machine. This flow must be suitably tuned, to minimize the amount of residuals being mixed with the new powder and to prevent oxidation due to oxygen exposure. From this point of view, it is clear that pausing production and opening the chamber door may have highly detrimental effects on the mechanical properties of the build parts. The parts being produced as closer as possible to the gas outlet are more protected against the oxidation mechanism, whereas those placed at the machine front side, close to the door, are more exposed. As a matter of the fact, some residuals are also visible as darker particles at the bottom side of Fig. 2, corresponding to the machine front side, involving also the sample contours and the built areas, where darker stripes can be observed. Therefore, a possible reason for the problems occurring mainly with Set #6 (S,3) is concerned with its location at the front side of the chamber, where it was even probably shadowed from the inert gas flow by the other parts. Similar defects and crack patterns as those in Fig. 9 (a, b) were observed in the other samples of the same set that experienced similar failures. The other ones that experienced correct failures exhibited regular crack surfaces. Most cracks started from porosities just beneath the surface (80 to 100 μm): an example (the initiation point is indicated by an arrow) is shown in Fig. 9 (c). Similar cracks, initiating from different size porosities, located just beneath the surface, have also been observed in [31], following fatigue cycling of Ti-6Al-4V.
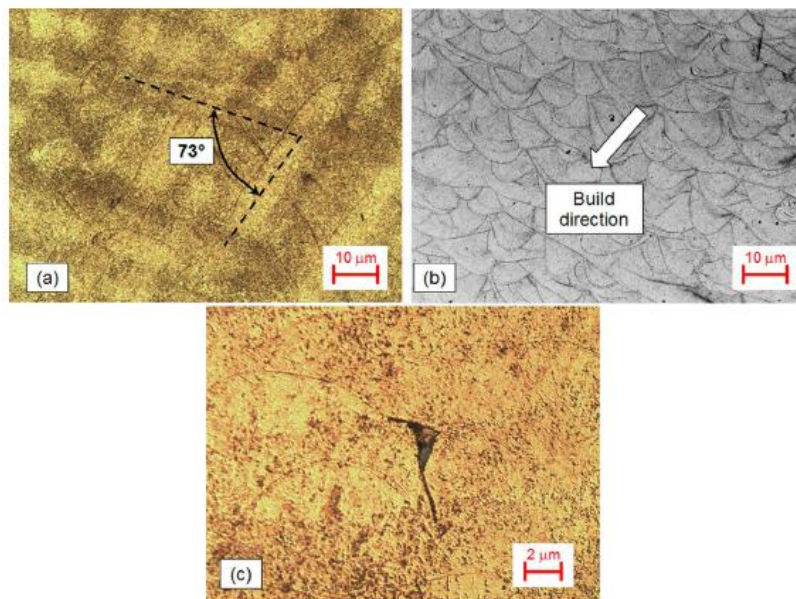

Fig. 10: Micrographic analyses on non-machined horizontally built samples: (a) laser scans on the build plane (contiguous planes are visible, relative angle highlighted), (b) layers along the stacking direction and (c) detail with an inclusion (images (a) and (c) post-processed by microscope filters and polarized lenses)

Regarding the structure upon the building process and the heat treatment, the laser scans in the build plane are shown in Fig. 10 (a). It can be emphasized that scans belonging to contiguous planes are overlapped in the same image, due to the very thin layer thickness (20 μm) and to an unavoidable slight alignment error. It makes it possible to estimate the relative angle, which is 73°, in agreement with the EOS Standard settings. The deposited layers are shown in Fig. 10 (b), where the section plane is along the stacking direction. The build orientation is embedded as well in the same picture. An inclusion is finally shown in Fig. 10 (c). Regarding Fig. 10, it can be pointed out that, despite heat treatments, the structure is

not made completely homogeneous: the scan layout and the layered structure are still well visible, which may justify the anisotropic effect remarked above.

CONCLUSIONS

This study aims at defining the fatigue strength of 15-5 PH Stainless Steel manufactured by Direct Metal Laser Sintering machine. There is a lack of data concerning the fatigue response of Additive Manufacturing processed parts of the aforementioned stainless steel. In particular, the topic regarding the effect of allowance, i.e., the amount of thickness to be removed by machining, has never been investigated. Moreover, regarding the build orientation, the slanted one has been very rarely involved in an extensive experimental study. The following points are worth mentioning, concerning the performed experimentation and the achieved results.

- Six sample sets were manufactured: horizontally, vertically and 45° inclined (with respect to the base plate), built with uniform allowance and with an incremented allowance at specimen gage (manufactured as cylindrical parts). This experiment can therefore be regarded as a 3-by-2 plan, involving two factors with three and two levels. The fatigue tests led to the determination of both the sloping parts of *S-N* curves and of the fatigue limits.
- The results indicate that allowance has a significant effect at enhancing the fatigue response. Conversely, the build orientation does not have an effect, when just horizontal and vertical orientations are considered. However, this factor becomes significant, when slanted samples are included in the experiment: this orientation led to improved results.
- These results indicate that machining makes it possible to remove the irregularities and residual stresses induced by the additive process, which are mainly concentrated at the surface layers. Moreover, the slanted orientation has the effect of reducing the notch effect due to scan errors or to powder residuals (defects per layer) and of increasing the resistance against crack propagation due to the layered structure.
- Taking advantage of build orientation or removing the surface irregularities may lead to increments of the fatigue strength in the order of 20%. It is worth noticing that the optimization of these factors leads to a fatigue performance that is well comparable to that of wrought material (ratio between the fatigue limit and the ultimate tensile strength around 50%).
- Finally, fractography and micrography have shown that, despite heat treatments, the layered structure induced by the process is still well visible, which can explain the moderate effect of build orientation on fatigue.
- Further developments will include the investigation of the effects of heat and surface treatments, including also further materials in the study. Possible effects, in terms of the generation of oxidation spots and of voids, arising from the position of the parts in the build chamber will also be investigated.

ACKNOWLEDGEMENTS

REFERENCES

1. Scott-Emuakpor O, Schwartz J, George T, Holycross C, Cross C, Slater J (2015). Bending fatigue life characterisation of direct metal laser sintering nickel alloy 718. *Fatigue Fract. Eng. Mater. Struct.*, 38, 1105-1117.

2. Abe F, Osakada K, Shiomi M, Uematsu K, Matsumoto M (2001). The manufacturing of hard tools from metallic powders by selective laser melting. *J. Mater. Process. Tech.*, 111, 210-213.

3. Rafi HK, Starr TL, Stucker BE (2013). A comparison of the tensile, fatigue, and fracture behaviour of Ti–6Al–4V and 15-5 PH stainless steel parts made by selective laser melting. *Int. J. Adv. Manuf. Tech.*, 69, 1299-1309.

4. Santos E, Masanari S, Osakada K, Laoui T (2006). Rapid manufacturing of metal components by laser forming. *Int. J. Mach. Tool Manu.*, 46, 1459-1468.

5. Herderick E (2011). Additive Manufacturing of Metals: A Review. *In Proc. of Materials Science and Technology (MS&T)*, October 16-20, 2011, Columbus, Ohio.

6. Razavi SMJ, Ferro P, Berto F, Torgersen J (In Press). Fatigue strength of blunt V-notched specimens produced by selective laser melting of Ti-6Al-4V. *Theor. Appl. Fract. Mec.*, DOI: 10.1016/j.tafmec.2017.06.021.

7. Vilaro T, Colin C, Bartout JD (2011). As-fabricated and heat-treated microstructures of the Ti-6Al-4V alloy processed by selective laser melting, *Metall. Mater. Trans. A*, 42A (10), 3190-3199.

8. Yang L, Gu H, Lassell A (2014). Surface treatment of Ti6al4V parts made by powder bed fusion additive manufacturing processes using electropolishing. *Proceedings of Solid Freeform Fabrication (SFF) Symposium*, Austin, TX.

9. Lewandowski JJ, Seifi M (2016). Metal Additive Manufacturing: A Review of Mechanical Properties. *Annu. Rev. Mater. Res.*, 46, 151-186.

10. Edwards P, Ramulu M (2014). Fatigue performance evaluation of selective laser melted Ti-6Al-4V. *Mat. Sci. Eng. A-Struct.*, 598, 327-337.

11. Edwards P, Ramulu M (2015). Effect of build direction on the fracture toughness and fatigue crack growth in selective laser melted Ti-6Al-4V. *Fatigue Fract. Eng. Mater. Struct.,* 38, 1228-1236.

12. Croccolo D, De Agostinis M, Fini S, Olmi G, Vranic A, Ciric-Kostic S (2016). Influence of the build orientation on the fatigue strength of EOS maraging steel produced by additive metal machine. *Fatigue Fract. Eng. Mater. Struct.*, 39, 637-647.

13. Abdelshehid M, Mahmodieh K, Mori K, Chen L, Stoyanov P, Davlantes D, Foyos J, Ogren J, Clark R Jr., Es-Said OS (2007). On the correlation between fracture toughness and precipitation hardening heat treatments in 15-5PH Stainless Steel. *Eng. Fail. Anal.*, 14, 626-631.

14. Muthupandi V, Bala Srinivasan P, Shankar V, Seshadri SK, Sundaresan S (2005). Effect of nickel and nitrogen addition on the microstructure and mechanical properties of power beam processed duplex stainless steel (UNS 31803) weld metals. *Mater. Lett.*, 59, 2305-2309.

15. You WD, Lee JH, Shin SK, Choe BH, Paik U, Lee JH (2005). Embrittlement fracture in a 17-4 PH stainless steel after aging at 400°C, *Mater. Sci. Forum*, 486-487, 241-244.

16. Byun TS, Yang Y, Overman NR, Busby JT (2016). Thermal Aging Phenomena in Cast Duplex Stainless Steels. *JOM*, 68, 507-516.

17. http://www.eos.info/material-m

18. Ozbaysal K, Inal OT (1994). Age-hardening kinetics and microstructure of PH 15-5 stainless steel after laser melting and solution treating. *J. Mater. Sci.*, 29, 1471-1480.

19. Palanisamy D, Senthil P, Senthilkumar V (2016). The effect of aging on machinability of 15Cr–5Ni precipitation hardened stainless steel. *Arch. Civ. Mech. Eng.*, 16, 53-63.

20. Wu J, Lin C (2002). Tensile and fatigue properties of 17-4 PH stainless steel at high temperatures. *Metall. Mater. Trans. A*, 33, 1715-1724.

21. Yadollahi A, Shamsaei N, Thompson SM, Elwany A, Bian L (2017). Effects of building orientation and heat treatment on fatigue behavior of selective laser melted 17-4 PH stainless steel. *Int. J. Fatigue*, 94, 218-235.

22. Taminger KMB, Hafley RA, Fhringer DT, Martin RE (2004). Effect of surface treatment on electron beam freeform fabricated aluminum structures. *Solid Freeform Fabrication Symposium*, Austin, TX.

23. Frank MC, Joshi A, Anderson DD, Thomas TP, Rudert MJ, Tochigi Y, Marsh JL, Brown TD (2010). Patient-specific bone implants using subtractive rapid prototyping. *Solid Freeform Fabrication Symposium*, Austin, TX.

24. MiroTek Finishing. www.microtekfinishing.com.

25. Rossi S, Deflorian F, Venturini F (2004). Improvement of surface finishing and corrosion resistance of prototypes produced by direct metal laser sintering. *J. Mater. Process. Technol.*, 148, 301-309.

26. Vaithilingam J, Goodridge RD, Christie SD, Edmondson S, Hague RJM (2012). Surface modification of selective laser melted structures using self-assembled monolayers for biomedical applications. Polishing. *Solid Freeform Fabrication Symposium*, Austin, TX.

27. Samoya M, Cormier D, Harrysson O, Cansizoglu O (2009). Mechanical properties of chemically milled titanium lattice structures. *Graduate Student Symposium*, North Carolina State Univesity.

28. Zhang X, Martina F, Ding J, Wang X, Williams S (2017). Fracture Toughness and Fatigue Crack Growth Rate Properties in Wire + Arc Additive Manufactured Ti-6Al-4V. *Fatigue Fract. Eng. Mater. Struct.*, 40 (5), 790-803.

29. Zhang J, Wang X, Paddea S, Zhang X (2016). Fatigue crack propagation behaviour in wire+arc additive manufactured Ti-6Al-4V: effects of microstructure and residual stress. *Mater. Des.*, 90, 551-561.

30. Van Hooreweder B, Moens D, Boonen R, Kruth J-P, Sas P (2012). Analysis of fracture toughness and crack propagation of Ti-6Al-4V produced by selective laser melting. *Adv. Eng. Mater.*, 14, 92-97.

31. Wycisk E, Siddique S, Herzog D, Walther F, Emmelmann C (2015). Fatigue performance of laser additive manufactured Ti-6A-4V in very high cycle fatigue regime up to 10^9 cycles, *Front. Mater.*, 2, article 72.

32. Brandl E, Heckenberger U, Holzinger V, Buchbinder D (2012). Additive manufactured AlSi10Mg samples using Selective Laser Melting (SLM): Microstructure, high cycle fatigue, and fracture behaviour. *Mater. Des.*, 34, 159-169.

33. Mower TM, Long MJ (2016). Mechanical behaviour of additive manufactured, powder-bed laser-fused materials, *Mat. Sci. Eng. A-Struct.*, 651, 198-213.

34. International Organization for Standardization ISO 1143:2010 (2010). *Standard - Metallic materials – Rotating bar bending fatigue testing*. International Organization for Standardization (ISO), Geneva, Switzerland.

35. Croccolo D, De Agostinis M, Olmi G (2013). Experimental characterization and analytical modelling of the mechanical behaviour of fused deposition processed parts made of ABS-M30. *Comput. Mater. Sci.*, 79, 506-518.

36. Maskery I, Aboulkhair NT, Corfield MR, Tuck C, Clare AT, Leach RK, Wildman RD, Ashcroft IA, Hague RJM (2016). Quantification and characterisation of porosity in selectively laser melted Al-Si10-Mg using X-ray computed tomography. *Mater. Charact.*, 111, 193-204.

37. Brown DW, Bernardin JD, Carpenter JS, Clausen B, Spernjak D, Thompson JM (2016). Neutron diffraction measurements of residual stress in additively manufactured stainless steel, *Mat. Sci. Eng. A-Struct.*, 678, 291-298.

38. Kruth J-P, Deckers J, Yasa E, Wauthlé R (2012). Assessing and comparing influencing factors of residual stresses in selective laser melting using a novel analysis method. *Proc. IMechE Part B: J. Engineering Manufacture*, 226, 980-991.

39. Casavola C, Campanelli SL, Pappalettere C (2008). Experimental analysis of residual stresses in the selective laser melting process. *Proceedings of the XI International Congress and Exposition*, June 2-5, 2008, Orlando, Florida, USA.

40. Benghalia G, Wood J (2016). Material and residual stress considerations associated with the autofrettage of weld clad components. *Int. J. Pres. Ves. Pip.*, 139-140, 146-158.

41. Kalentics N, Boillat E, Peyre P, Ciric-Kostic S, Bogojevic N, Logé RE (2017). Tailoring residual stress profile of Selective Laser Melted parts by Laser Shock Peening. *Additive Manufacturing*, 16, 90-97.

42. Fergani O, Berto F, Welo T, Liang SY (2017). Analytical modelling of residual stress in additive manufacturing. *Fatigue Fract. Eng. Mater. Struct.*, 40, 971-978.

43. Olmi G, Freddi A (2013). A new method for modelling the support effect under rotating bending fatigue: Application to Ti-6Al-4V alloy, with and without shot peening. *Fatigue Fract. Eng. Mater. Struct.*, 36 (10), 981-993.

44. Dixon WJ, Massey F Jr. (1983). *Introduction to Statistical Analysis*. McGraw-Hill, New York, United States.

45. Olmi G, Comandini M, Freddi A (2010). Fatigue on shot-peened gears: Experimentation, simulation and sensitivity analyses. *Strain*, 46 (4), 382-395.

46. Van Hooreweder B, Moens D, Boonen R, Sas P (2012). The critical distance theory for fatigue analysis of notched aluminium specimens subjected to repeated bending. *Fatigue Fract. Eng. Mater. Struct.*, 35, 878-884.

47. International Organization for Standardization ISO 12107:2012 (2012). *Metallic Materials – Fatigue Testing – Statistical Planning and Analysis of Data*. International Organization for Standardization (ISO), Geneva, Switzerland.

48. ASM International (2016). *ASM Handbook*. Vol. 1, Materials Park, Ohio.

49. ASM International (2016). *ASM Handbook*. Vol. 2, Materials Park, Ohio.

50. Croccolo D, De Agostinis M, Olmi G (2013). Fatigue Life Characterisation of Interference Fitted Joints. *In: Volume 2B: Advanced Manufacturing, p. 106-116, ASME - American Society of Mechanical Engineers*, ISBN: 9780791856192, San Diego (CA, United States), November 15-21, 2013, DOI: 10.1115/IMECE2013-63515.

51. Croccolo D, De Agostinis M, Fini S, Morri A, Olmi G (2014). Analysis of the Influence of Fretting on the Fatigue Life of Interference Fitted Joints. *In: Volume 2B: Advanced Manufacturing. p. 1-10, ASME - American Society of Mechanical Engineers*, ISBN: 9780791846445, Montreal, Canada, 14-20 November, 2014, DOI: 10.1115/IMECE2014-38128.

52. Olmi G (2012). Low Cycle Fatigue Experiments on Turbogenerator Steels and a New Method for Defining Confidence Bands. *J. Test. Eval.*, 40, 4, Paper ID JTE104548.

53. Croccolo D, De Agostinis M, Fini S, Olmi G (2016). Influence of the engagement ratio on the shear strength of an epoxy adhesive by push-out tests on pin-and-collar joints: Part I: Campaign at room temperature. *Int. J. Adhes. Adhes.*, 67, 69-75.

54. Croccolo D, De Agostinis M, Fini S, Olmi G (2016). Influence of the engagement ratio on the shear strength of an epoxy adhesive by push-out tests on pin-and-collar joints: Part II: Campaign at different temperature levels. *Int. J. Adhes. Adhes.*, 67, 76-85.

55. Niemann G, Winter H, Hohn BR (2005). *Maschinenelemente*. Springer-Verlag, Berlin, Germany.

56. Weingarten C. Buchbinder D, Pirch N, Meiners W, Wissenbach K, Poprawe R (2015). Formation and reduction of hydrogen porosity during selective laser melting of AlSi10Mg. *J. Mater. Process. Technol.*, 221, 112-120.

57. Simonelli M, Tuck C, Aboulkhair NT, Maskery I, Ashcroft I, Wildman RD, Hague RJM (2015). A study on the laser spatter and the oxidation reactions during selective laser melting of 316L stainless steel, Al-Si10-Mg and Ti-6Al-4V. *Metall. Mater. Trans. A*, 46, 3842-3851.